Imaging of Tumor-Associated Vascular Prostate-Specific Membrane Antigen in Woodchuck Model of Hepatocellular Carcinoma

Olga Sergeeva[1], **Yifan Zhang**[1], **Willian Julian**[1], **Arun Sasikumar**[2], **Amad Awadallah**[3], **Jonathan Kenyon**[1], **Wuxian Shi**[4], **Maxim Sergeev**[5], **Steve Huang**[6], **Sandra Sexton**[7], **Renuka Iyer**[7], **Wei Xin**[3], **Norbert Avril**[5], **Ernest Ricky Chan**[8], **Zhenghong Lee**[1]

[1]Radiology, Case Western Reserve University, Cleveland, Ohio;

[2]Nuclear Medicine, St. Gregorios International Cancer Care Centre, Parumala, Kerala, India;

[3]Pathology, University Hospitals Cleveland Medical Center, Cleveland, Ohio;

[4]Center for Proteomics and Bioinformatics, Case Western Reserve University, Cleveland, Ohio;

[5]Radiology, University Hospitals Clevel and Medical Center, Cleveland, Ohio;

[6]Nuclear Medicine, Cleveland Clinic, Cleveland, Ohio;

[7]Medical Oncology, Roswell Park Cancer Institute, Buffalo, New York;

[8]Institute for Computational Biology, Case Western Reserve University, Cleveland, Ohio

Abstract

BACKGROUND AND AIMS: Radiolabeled short peptide ligands targeting prostate-specific membrane antigen (PSMA) were developed initially for imaging and treatment of prostate cancers.

While many nonprostate solid tumors including hepatocellular carcinoma (HCC) express little PSMA, their neovasculature expresses a high level of PSMA, which is avid for Gallium-68-labeled PSMA-targeting radio-ligand (^{68}Ga-PSMA-11) for positron emission tomography (PET). However, the lack of a spontaneous animal model of tumor-associated vascular PSMA overexpression has hindered the development and assessment of PSMA-targeting radioligands for imaging and therapy of the nonprostatic cancers. We identified detectable indigenous PSMA expression on tumor neovascular endothelia in a naturally occurring woodchuck model of HCC.

METHODS: Molecular docking was performed with 3 bait PSMA ligands and compared between human and woodchuck PSMA. Initially, PET images were acquired dynamically after intravenously injecting 37 MBq (1.0 mCi) of ^{68}Ga-PSMA-11 into woodchuck models of HCC. Subsequently, 10-minute static PET scans were conducted for other animals 1-hour after injection due to HCC and liver background uptake stabilization at 30–45 minutes after injection. Liver tissue samples were harvested after imaging, fresh-frozen for quantitative reverse transcription polymerase chain reaction and western blot for validation, or fixed for histology for correlation.

RESULTS: Our preclinical studies confirmed the initial clinical findings of ^{68}Ga-PSMA-11 uptake in HCC. The agents (ligands and antibodies) developed against human PSMA were found to be reactive against the woodchuck PSMA.

CONCLUSION: This animal model offers a unique opportunity for investigating the biogenesis of tumor-associated vascular PSMA, its functional role(s), and potentials for future treatment strategies targeting tumor vascular PSMA using already developed PSMA-targeting agents.

Introduction

With its overexpression on the surface of prostate cancer cells and its extracellular binding pocket for small-molecule ligands, prostate-specific membrane antigen (PSMA) appears to be an effective target for imaging detection and targeted therapy of prostate cancers.[1] PSMA is also known as glutamate carboxypeptidase II (GCP II, in the brain) or *N*-acetylated-alpha-linked-acidic dipeptidase, which hydrolyzes the terminal a-linked glutamate from neuropeptide N-acetyl-Asp-Glu (NAAG) and folate hydrolase 1 (along the gastrointestinal tract), which hydrolyzes the γ-linked terminal glutamates from polyglutamated folates. In fact, targeting PMSA for imaging and treatment of prostate cancer has been an active field of development with many groups working on similar PSMA-targeting radioligands.[2–9] These ligands, mostly Glu-urea-Lys or urea-based, would bind to the binding pocket of PSMA with high binding affinity like the endogenous (native) ligands, but would not be cleaved by the enzymatic activities of PSMA due to the substitution with urea. Two of them recently obtained regulatory approval for human use, both urea-based short peptides either conjugated via the acyclic radiometal chelator HBED-CC to the radioisotope Gallium-68, [^{68}Ga]PSMA-HBED-CC (short for [^{68}Ga]PSMA-11), or directly labeled with fluorine-18 (F-18) as the small molecule [^{18}F]DCFPyL. [^{68}Ga]PSMA-11 has been used extensively first in Europe and then at other places for positron emission tomography (PET) imaging of

prostate cancer[10–13] and has gained approval from the US Food and Drug Administration for PET imaging of PSMA-positive lesions in men with prostate cancer.[14] Similarly, [18F]DCFPyL obtained US Food and Drug Administration approval for PET imaging to identify suspected metastasis or recurrence of prostate cancer.[15]

Besides prostate cancer, PSMA is recognized for its overexpression in the neovasculature associated with nonprostatic solid tumors such as brain, breast, head and neck, and several other cancers,[16–20] making it a general biomarker for a wide spectrum of cancers even though many of these tumors including primary liver cancer hepatocellular carcinoma (HCC) do not express PSMA. Since blood vessels in normal tissues express little or no PSMA,[16] this tumor-associated vascular endothelium overexpression of PSMA is clearly an ideal molecular target for cancer imaging in general and vascular-oriented treatment. Incidental clinical findings[21,22] on high uptake of [68Ga]PSMA-11 in HCC during PET imaging were replicated independently[23,24] including ours as shown in Figure A1. The literature pointed to tumor-associated vascular PSMA that was overexpressed in HCC and responsible for [68Ga]PSMA-11 uptake during PET imaging. However, the induction of overexpression and the function(s) of this tumor vascular PSMA were not entirely clear.[25] Investigation on the subject has not progressed satisfactorily in the past due mainly to the lack of a suitable model system. Preclinical investigations of vascular expression of PSMA in normal and tumor tissues in lab mice have proven difficult. For example, PSMA was not detected by a rat monoclonal antibody (mAb), which recognizes both mouse and human PSMA, on the vessels of any tumors grown in mice, regardless of the type of tumor, site of implantation, or tissue of origin.[26] Despite being a promising vascular target, PSMA has not been fully explored in the absence of endothelial model systems that overexpress PSMA either in vitro or in animal tumor models.

We discovered a detectable level of animal's native PSMA on tumor-associated vascular endothelium of a clinically relevant animal model of HCC in the woodchuck (*Marmota monax*), which is featured by chronic infection with the woodchuck hepatitis virus, homologous to human hepatitis B virus. This model has been used for developing antiviral treatments[27–30] as well as cancer imaging.[31] We have been conducting PET imaging studies for evaluating a list of PET imaging radioligands[32] against the endogenous woodchuck targets (homologs to the same targets in human) with this naturally occurring woodchuck model of HCC without implanting human tissues/fluids or introducing chemical agents/ toxins. The short peptide ligands designed to target human PSMA and the antibody developed to stain human PSMA were found to be reactive with the native woodchuck vascular PSMA associated with the spontaneously developed HCC in the woodchucks. This manuscript presents the preliminary findings from PET imaging of tumor-associated vascular PSMA in woodchuck HCC using the already developed clinical PET radioligand against PSMA. This animal model offers a unique opportunity for investigating the biogenesis of tumor-associated vascular PSMA, its functional role(s), and its potential clinical utilities such as possible HCC treatment strategies targeting tumor vascular PSMA.

Materials and Methods

Animal Models

Four woodchucks weighed 8–10 lbs (averaged 3.5 kg) and aged 2–4 years were selected at the Roswell Park Comprehensive Cancer Center (Buffalo, NY) once their liver lesion reached 2 cm in diameter as determined by ultrasound for shipment to the Case Western Reserve University (Cleveland, OH). One age-matched control without tumors was also shipped. A venous access port (SAI Infusion Technologies, Lake Villa, IL) was surgically implanted in each animal to facilitate radiotracer injection in all PET scans. The port was flushed regularly with heparinized saline. The food was taken away 4–5 hours before each PET imaging session to ease the anesthesia procedure while drinking water was not restricted. All procedures were approved by the Institutional Animal Care and Use Committee and the Radiation Safety Committee of the University.

Bioinformatics

Homology of amino acid (a.a.) sequences between human (*Homo sapiens*) and woodchuck (*Marmota monax*) PSMA was determined by using a Protein Basic Local Alignment Search Tool (https://blast.ncbi.nlm.nih.gov/Blast.cgi). The 2 species were searched for their sequences of folate hydrolase 1 (National Center for Biotechnology Information Reference Sequence: NP_004467.1 [*Homo sapiens*]; National Center for Biotechnology Information Reference Sequence: KAF7476917.1 [*Marmota monax*]) for homology analysis. The woodchuck genome has not been completely sequenced, and KAF7476917.1 is a hypothetical predicted protein sequence for woodchuck PSMA based on the analysis of the woodchuck biosample (liver tissue).

SWISS-MODEL

There are no 3D protein structures for woodchuck PSMA deposited in the protein database (PDB). Therefore, SWISS-MODEL (https://swissmodel.expasy.org/interactive), a Web-based integrated service dedicated to protein structure homology modeling,[33] was used to guide us in building protein homology models for woodchuck PSMA. A high-resolution (1.4 Å) crystal structure analysis for homology modeling with SWISS-MODEL was performed. The a.a. sequence of the target protein, KAF7476917.1, was used as an input. The automatic pipeline identified a list of suitable templates based on Basic Local Alignment Search Tool and HHblits[34] to generate a 3D protein structure of woodchuck PSMA. The 2 woodchuck 3D protein models were selected from the list generated based on the top-ranked templates of human PSMA deposited in PDB; 3BXM, structure of an inactive mutant of human GCP II combined with the native ligand NAAG, and 4P4E, X-ray structure of human GCP II combined with a phosphoramidate ligand MP1D. An additional woodchuck 3D protein model was generated based on a specified human PSMA template; 5O5T, X-ray structure of human GCP II combined with a urea-based inhibitor PSMA-1007. The generated 3D homologous models were saved in PDB format for docking and display.

Molecular Docking

Docking was performed using the GOLD software from Cambridge Crystallographic Data Centre (https://www.ccdc.cam.ac.uk). Protein structures were accessed from the Research Collaboratory for Structural Bioinformatics PDB database for human PSMA or generated using SWISS-MODEL as mentioned above for woodchuck PSMA. Bait ligands (NAAG, MP1D, and PSMA-1007) were obtained from the Research Collaboratory for Structural Bioinformatics PDB database or generated through ChemDraw (PerkinElmer Informatics, Waltham, MA). Ligand editing was performed using the HERMES software package also from Cambridge Crystallographic Data Centre.

Each individual ligand was docked according to the developer's guidelines using 20 runs of the general algorithm, with 100,000 operations per run. To maintain a level of diversity in the docking positions, docking was performed both with and without the diverse solutions option. The minimal root mean square deviation of the diverse solutions was set to 1.5A. Docking was preformed using ligands with physiologic protonation states, and all solute water molecules were removed. Protein structures were fully protonated according to developer's guidelines. The CHEMPLP scoring function includes a combination of energy terms from both the CHEM-SCORE as well as the Piecewise linear potential scoring functions.[35]

Radiotracers

For PET imaging, [^{68}Ga]PSMA-11, a urea-based ligand, was synthesized automatically with the Scintomics module (Fürstenfeldbruck, Germany) with prepared cassettes and using the sequences provided by the vendor.

Imaging Experiments and Data Analysis

For each scan, the animal was placed prone in the clinical ingenuity PET/computed tomography (CT) scanner (Philips, Cleveland, OH) and under 3% isoflurane gas anesthesia throughout the scan. After a low-dose CT scan, 52–80 MBq (1.46–2.1 mCi) of [^{68}Ga]PSMA-11 was injected intravenously through the implanted venous access port and followed by a dynamic PET scan of 60 minutes in list mode on the Philips PET/CT system. The woodchucks with an average weight of 3.5 kg would not fit into the micro-PET. PET acquisition was rebinned into a total of 21 frames: 10×30-second, 5×1-minute, 2×5-minute, and 4×10-minute frames, respectively. After the initial batch, animals were scanned 55 minutes after injection with 10-minute static scan based on tracer kinetic analysis. After the experiment, the animals were euthanized for tissue harvesting. Some of the tissue samples were fixed for histology while others were fresh-frozen immediately for later use in real-time quantitative reverse transcription polymerase chain reaction (qRT-PCR) or western blot.

Standardized uptake value (SUV), which is the normalized radiotracer uptake by body weight and injected dose,[36] was calculated based on the circular regions of interest placed in the liver as well as focal uptakes of the tumors, and time activity curves in the unit of SUV were generated for these regions of interest.

Histology

Fixed issue samples were embedded in paraffin blocks, and adjacent slides were cut and deparaffinized for hematoxylin and eosin (H&E) staining and immunohistochemical staining with mouse mAb against human PSMA (1:200 dilution, Catalog #NCL-L-PSMA, clone 1D6 from Leica Biosystems, Newcastle, United Kingdom).

Quantitative Reverse Transcription Polymerase Chain Reaction

RNA was extracted from the frozen tissue using a Qiagen miRNeasy Mini Kit (Cat. No.217004) according to manufacturer's instructions. Total RNA (0.1 μg for each reaction) was used to generate complementary DNA (cDNA) with the High-Capacity RNA-to-cDNA Kit (Cat. No. 4387406; Applied Bio-systems). The primers for qRT-PCR were designed using the Custom TaqMan Assay Design Tool based on marmot mRNA sequences for required genes: PSMA (based on XP_015332802.1) and endogenous control gene GAPDH (based on XM_015500718.1). qRT-PCR Was performed on a StepOne Plus real-time thermocycler with 1.33 mL of cDNA for each reaction and the TaqMan Universal master Mix II, with UNG (Cat. No. 4440038; Applied Biosystems). Expression data were obtained for each gene from each sample as threshold cycle (Ct).　Ct was calculated as the Ct of endogenous control gene minus the Ct of the gene of interest.　　Ct was then calculated as the　Ct of the reference sample minus the　Ct of another sample. The relative quantification of gene expression was calculated as $2^{-(\text{Ct})}$.

Western Blot

The frozen animal tissue samples were homogenized using pestle mortar method and were then added into the radio-immunoprecipitation assay buffer. The homogenized samples were passed 2–3 times through a 25G needle, and after that the samples were incubated for 1 hour on ice and were then centrifuged for 30 minutes at 28,000 $\times$ g at 4 °C to remove any remaining insoluble material. The supernatant was used for western blot analysis, while the pellet was discarded. Protein content was determined using BCA Protein Assay Kit (# 23225; Thermo Fisher Scientific) according to manufacturer's instructions. For western blot analysis, 20 μg of protein was tested for loading into 7.5% precast polyacrylamide gel (Bio Rad) analyzed by sodium dodecyl sulfate–polyacrylamide gel electrophoresis and transferred onto a polyvinylidene difluoride membrane using an iBlot Dry blotting system (Invitrogen). The membranes were incubated in blocking buffer overnight followed by incubation with mouse anti-PSMA antibody (ab76104; Abcam) in 5% nonfat dry milk in TBS at 1:1000. The blots were washed thrice in tris-buffered saline containing 0.1% Tween-20 for 5 minutes each followed by incubation with peroxidase-conjugated goat antimouse secondary antibody in 1:1000 dilution. β-Actin (D6A8) rabbit mAb (Cell Signaling Technology) were used as an endogenous control at 1:1000 dilution following peroxidase-conjugated goat antirabbit secondary antibody at 1:2000 dilution. Finally, blots were washed in tris-buffered saline containing 0.1% Tween-20 and developed with ECL chemiluminescent detection reagent (Cytiva Amersham). Chemiluminescence signals were visualized using the exposure film.

Results

Genome blast between human and woodchuck (marmot) PSMA showed 100% homology from exon 1 to exon 4 between the human and woodchuck PSMA. The protein sequence (FASTA) also showed high (89%) identity between human and woodchuck PSMA (Figure A1A). Using the SWISS-MODEL for homologous modeling, we were able to dock the native ligand such as the neuropeptide NAAG as well as the radioligands to the binding site in PSMA for both the human and woodchuck proteins (Figure 1). In addition, the a.a. residues *Glu424*, *Tyr552*, *Asn519*, *Arg210*, *Arg536*, *Arg534*, and *Arg463* (the so-called *arginine patch*), as well as other a.a. residues in the vicinity of this binding pocket that have functional structures, were found to be preserved between humans and woodchucks as shown in Figure A2B.

Docking scores were computed using the ChemPLP scoring function, which is an empirical scoring function built upon the Protein-Ligand ANT system algorithm which relies upon weighted energy terms to approximate the binding affinity between the protein and substrate. Table presented the comparison of docking scores of 3 small-molecule PSMA ligands docked into the protein structures of human and woodchuck PSMAs. In column #1, the endogenous ligand NAAG was docked into the 3D protein structure 3BXM (that was determined in a binding complex with NAAG) for human PSMA as well as a homologous woodchuck PSMA protein structure modeled using the human 3BXM as its template. In column #2, a small phosphoramidate ligand 2-(phosphonomethyl)-pentandioic acid was docked into the protein structure 4P4E (that was determined in a blinging complex with another phosphoramidate ligand MP1D) for human PSMA and a homologous woodchuck protein structure modeled after 4P4E. In column #3, a small urea-based F-18-labeled radioligand [^{18}F]DCFPyL was docked into the 5O5T (that was determined in a binding complex with another F-18-labeled urea-based ligand [^{18}F]PSMA-1007) for human PSMA and a homologous woodchuck structure modeled after 5O5T. The docking scores are consistently comparable between humans and woodchucks although the woodchuck scores were slightly lower in each column most probably due to the nature of the homologous protein models used since no protein structures of woodchuck PSMA have been submitted.

PET scans using [^{68}Ga]PSMA-11 with the woodchuck models of HCC showed regional quantification of radiotracer uptake, in terms of SUV, in liver cancer. Figure 2A demonstrates the sustained uptake of [^{68}Ga]-PSMA-11 in HCC at 1 hour after injection of the radiotracer, and again 5 hours later. The scan of a control animal without HCC at 1 hour after injection was also displayed in comparison. Figure 2B showed a typical time-activity curve of the radiotracer up-take, obtained during the initial 60-minute dynamic PET scan, in which the SUV plateaued at 4.0 in HCC after 30–40 minutes while the liver background SUV dropped below 2.0, suggesting a favorable time window around that time span after injection for a suitable static PET scan for the radio-tracer uptake in liver cancer. Longitudinal tracking by PET imaging was also performed for some animals showing a steady tracer uptake in the tumor despite of the progression of HCC in size. The tumor SUV remained at similar levels 100 days apart, which is approximately 1.5 woodchuck years, when the tumor increased from 2.5 cm to 4.7 cm along the long axis (Figure 2C).

Histological staining was performed with tissue samples harvested after imaging for correlation with the imaging results. H&E staining was shown in Figure 3A indicating mostly moderately differentiated HCCs. The mouse mAb against human PSMA used for immunohistochemical staining revealed positive microvascular PSMA staining within the woodchuck HCC as shown in Figure 3B corroborating that the existing [^{68}Ga]-PSMA ligand developed for imaging human PSMA positively depicted native woodchuck vascular PSMA associated with its HCC in this spontaneous animal model. The woodchuck liver without HCC was also stained with the same H&E and PSMA as a control.

Harvested tumor tissues were processed for western blot using the mouse mAb against human PSMA. Figure 4 (top) presents the positive western blotting results from HCC1 (**1**), HCC2 (**2**), and HCC3 (**3**) compared to liver tissues from the liver of the carrier with HCC3 (**4**), normal control (**5**), and tumor margin of the carrier with HCC3 (**6**), further demonstrating that reagents developed against human PSMA are applicable toward woodchuck PSMA. PCR results (Figure 4, bottom) showed that tumor tissue PSMA expression was 1.7- to 3.1-fold higher than that in normal liver. The questionable tissues between the tumor and liver were designated as the "Margin", which was also used for western blot (above). However, kidney sample showed the highest PSMA expression (3.6- to 6.1-fold increase from the liver). Not all animals had margin tissues collected, and only some animals had kidney tissues collected during tissue harvest.

Discussion

Currently, clinical diagnosis of HCC depends heavily on imaging with contrast-enhanced CT or magnetic resonance imaging angiography for detecting the typical vascular flow patterns.[37] However, some primary liver cancers such as HCC do not show the "typical" vascular flow pattern,[38] while other nontumor hepatic lesions and benign liver tumors are also hypervascular.[39] Radiological findings, therefore, are often supplemented by biopsies for subsequent histopathology confirmation. PET may offer an alternative provided an appropriate PET radiotracer is available. Unfortunately, PET imaging using the commonly available glucose analog [^{18}F]fluorodeoxyglucose (FDG), which measures increased cellular glucose metabolism and has dramatically improved patient management in a large variety of cancers, has severe limitations for imaging primary liver cancers such as HCC due to a high false-negative rate as many HCCs have relatively low FDG uptake.[40] The ability of FDG-PET to depict extrahepatic lesions metastasized from HCC is also doubtful as shown in Figure A1. Other PET imaging markers of HCC are sought after.

The preclinical PET scans presented in Figure 2 confirmed the clinical findings on the uptake of [^{68}Ga] PSMA-11 in HCC. PSMA is conserved enough between humans and woodchucks in terms of ligand binding (Figure 1, Table and Figure A2) allowing further investigation into the possibility of "repurposing" this class of developed prostate cancer radioligands for PET imaging of tumor-associated neovasculature through the spontaneous woodchuck model of HCC. Compared to other small-molecule PET tracers that have been tested for liver cancer imaging, PSMA-targeting imaging is vascular centric as HCC tumor cells do not express PSMA (Figure 3). Approximately, only up to 15% of the harvested liver tissues contain endothelial cells,[41] and those associated with HCC are a further fraction.

This may explain the slightly lower than expected intensity in western blot and relative quantification of gene expression values from the PCR (Figure 4). The liver has a baseline PSMA expression, but at a much lower level than HCC (Figure 4), which corroborated the low background uptake of the PSMA radiotracer in the liver (Figure 2).

The strong kidney uptake was noticed in both woodchuck and human scans, and PCR also showed a high renal expression of PSMA. Although renal cell carcinoma (RCC) is not the topic of this investigation, preliminary clinical experiences indicated the potential of PSMA-PET imaging for clinical staging of RCC,[42] especially for detecting metastatic RCC,[43] due to the much higher PSMA expression in RCC compared to the high baseline PSMA expression in the normal kidneys.

Although PSMA has been reported to be overexpressed in the neovasculature of many solid human tumors, the lack of spontaneous animal models has hindered the development and assessment of PSMA-targeted radioligands for imaging and therapy of human tumors other than prostate cancers. Investigations of neovascular PSMA expression were hampered as both tumor xenografts and patient-derived xenograft models (where the original human endothelial cells were replaced by the mouse counterparts after 1 passage) do not express native murine PSMA in tumor-associated vasculature.[44] It is unclear why murine tumor vascular endothelium lacks detectable expression of PSMA.[45]

We have identified insofar the woodchuck model of chronic viral infection-induced primary liver cancer HCC with detectable indigenous woodchuck PSMA on tumor-associated neovasculature. Although HCCs originated from etiologies other than HBV infection need to be looked into for a similar PSMA expression pattern, a range of studies with PSMA as a tumor vascular marker can be conducted with the woodchuck model of HCC for the biogenesis of its overexpression in primary liver cancer going through multistep but different processes, potentially in relation to stromal reaction as well as for its function(s). For example, tumor-associated vascular PSMA may play a role independent of major endothelium activator, vascular endothelial growth factor, in tumor angiogenesis.[46,47] The clinical utility of PET imaging with vascular targeting [68Ga]PSMA-11 for liver cancers is yet to be determined as trails are ongoing (NCT03983407, NCT04310540, NCT04762888). Perhaps, PET imaging with [68Ga]PSMA-11 can be incorporated in future clinical trials to identify liver cancer patients with vascular PSMA overexpression for better assessment of the response to PSMA-targeting therapies so as to supplement current standard clinical scans and also to reduce the frequency of invasive liver biopsies.

Supplementary Material

Refer to Web version on PubMed Central for supplementary material.

Funding:

Abbreviations used in this paper:

a.a.	amino acid
cDNA	complementary DNA
Ct	threshold cycle
CT	computed tomography
F-18	fluorine-18
FDG	[^{18}F]fluorodeoxyglucose
Ga-PSMA-11	[^{68}Ga]PSMA-HBED-CC
GCP II	glutamate carboxypeptidase II
H&E	hematoxylin and eosin
HCC	hepatocellular carcinoma
mAb	monoclonal antibody
NAAG	N-acetyl-Asp-Glu
PDB	protein database
PET	positron emission tomography
PSMA	prostate-specific membrane antigen
qRT-PCR	quantitative reverse transcription polymerase chain reaction
RCC	renal cell carcinoma
SUV	standardized uptake value

References

1. Wang X, Yin L, Rao P, et al. Targeted treatment of prostate cancer. J Cell Biochem 2007;102:571–579. [PubMed: 17685433]

2. Israeli RS, Powell CT, Corr JG, et al. Expression of the prostate-specific membrane antigen. Cancer Res 1994; 54:1807–1811. [PubMed: 7511053]

3. Wright GL Jr, Grob BM, Haley C, et al. Upregulation of prostate-specific membrane antigen after androgen-deprivation therapy. Urology 1996;48:326–334. [PubMed: 8753752]

4. Bostwick DG, Pacelli A, Blute M, et al. Prostate specific membrane antigen expression in prostatic intraepithelial neoplasia and adenocarcinoma: a study of 184 cases. Cancer 1998;82:2256–2261. [PubMed: 9610707]

5. Tasch J, Gong M, Sadelain M, et al. A unique folate hydrolase, prostate-specific membrane antigen (PSMA): a target for immunotherapy? Crit Rev Immunol 2001; 21:249–261. [PubMed: 11642607]

6. Mannweiler S, Amersdorfer P, Trajanoski S, et al. Heterogeneity of prostate-specific membrane antigen (PSMA) expression in prostate carcinoma with distant metastasis. Pathol Oncol Res 2009;15:167–172. [PubMed: 18802790]

7. Ross JS, Sheehan CE, Fisher HA, et al. Correlation of primary tumor prostate-specific membrane antigen expression with disease recurrence in prostate cancer. Clin Cancer Res 2003;9:6357–6362. [PubMed: 14695135]

8. Mitsiades CS, Lembessis P, Sourla A, et al. Molecular staging by RT-pCR analysis for PSA and PSMA in peripheral blood and bone marrow samples is an independent predictor of time to biochemical failure following radical prostatectomy for clinically localized prostate cancer. Clin Exp Metastasis 2004;21:495–505. [PubMed: 15679047]

9. Giesel FL, Hadaschik B, Cardinale J, et al. F-18 labelled PSMA-1007: biodistribution, radiation dosimetry and histopathological validation of tumor lesions in prostate cancer patients. Eur J Nucl Med Mol Imaging 2017; 44:678–688. [PubMed: 27889802]

10. Afshar-Oromieh A, Haberkorn U, Eder M, et al. [68Ga] Gallium-labelled PSMA ligand as superior PET tracer for the diagnosis of prostate cancer: comparison with 18F-FECH. Eur J Nucl Med Mol Imaging 2012;39:1085–1086. [PubMed: 22310854]

11. Afshar-Oromieh A, Malcher A, Eder M, et al. PET imaging with a [68Ga]gallium-labelled PSMA ligand for the diagnosis of prostate cancer: biodistribution in humans and first evaluation of tumour lesions. Eur J Nucl Med Mol Imaging 2013;40:486–495. [PubMed: 23179945]

12. Eder M, Schafer M, Bauder-Wust U, et al. 68Ga-complex lipophilicity and the targeting property of a urea-based PSMA inhibitor for PET imaging. Bioconjug Chem 2012;23:688–697. [PubMed: 22369515]

13. Schafer M, Bauder-Wust U, Leotta K, et al. A dimerized urea-based inhibitor of the prostate-specific membrane antigen for 68Ga-PET imaging of prostate cancer. EJNMMI Res 2012;2:23. [PubMed: 22673157]

14. Administration USFD. FDA approves first PSMA-targeted PET imaging drug for men with prostate cancer. Silverspring: United States Food and Drug Administration; 2020.

15. Morris MJ, Rowe SP, Gorin MA, et al. Diagnostic performance of (18)F-DCFPyL-PET/CT in men with biochemically recurrent prostate cancer: results from the CONDOR phase III, multicenter study. Clin Cancer Res 2021;27:3674–3682. [PubMed: 33622706]

16. Liu H, Moy P, Kim S, et al. Monoclonal antibodies to the extracellular domain of prostate-specific membrane antigen also react with tumor vascular endothelium. Cancer Res 1997;57:3629–3634. [PubMed: 9288760]

17. Chang SS, Reuter VE, Heston WD, et al. Five different anti-prostate-specific membrane antigen (PSMA) antibodies confirm PSMA expression in tumor-associated neovasculature. Cancer Res 1999;59:3192–3198. [PubMed: 10397265]

18. O'Keefe DS, Bacich DJ, Heston WD. Comparative analysis of prostate-specific membrane antigen (PSMA) versus a prostate-specific membrane antigen-like gene. Prostate 2004;58:200–210. [PubMed: 14716746]

19. Haffner MC, Kronberger IE, Ross JS, et al. Prostate-specific membrane antigen expression in the neovasculature of gastric and colorectal cancers. Hum Pathol 2009;40:1754–1761. [PubMed: 19716160]

20. Rajasekaran A, Anilkumar G, Christiansen JJ. Is prostate-specific membrane antigen a multifunctional protein? Am J Physiol Cell Physiol 2005;228:C975–C981.

21. Sasikumar A, Joy A, Nanabala R, et al. (68)Ga-PSMA PET/CT imaging in primary hepatocellular carcinoma. Eur J Nucl Med Mol Imaging 2016;43:795–796. [PubMed: 26743897]

22. Soyal C, Alkan A, Ozkan E, et al. Ga-68 PSMA accumulation in hepatocellular carcinoma. Clin Imaging 2016; 1:2.

23. Erhamamci S, Aslan N. Comparative findings between (68)Ga-PSMA and (18)F-FDG PET/CT for hepatocellular carcinoma. Mol Imaging Radionucl Ther 2020; 29:135–138. [PubMed: 33094578]

24. Kiess AP, Minn I, Chen Y, et al. Auger radiopharmaceutical therapy targeting prostate-specific membrane antigen. J Nucl Med 2015;56:1401–1407. [PubMed: 26182968]

25. Conway RE, Petrovic N, Li Z, et al. Prostate-specific membrane antigen regulates angiogenesis by modulating integrin signal transduction. Mol Cell Biol 2006; 26:5310–5324. [PubMed: 16809768]

26. Huang X, Bennett M, Thorpe PE. Anti-tumor effects and lack of side effects in mice of an immunotoxin directed against human and mouse prostate-specific membrane antigen. Prostate 2004;61:1–11. [PubMed: 15287089]

27. Menne S, Butler SD, George AL, et al. Antiviral effects of lamivudine, emtricitabine, adefovir dipivoxil, and tenofovir disoproxil fumarate administered orally alone and in combination to woodchucks with chronic woodchuck hepatitis virus infection. Antimicrob Agents Chemother 2008;52:3617–3632. [PubMed: 18676881]

28. Menne S, Tumas DB, Liu KH, et al. Sustained efficacy and seroconversion with the toll-like receptor 7 agonist GS-9620 in the woodchuck model of chronic hepatitis B. J Hepatol 2015;62:1237–1245. [PubMed: 25559326]

29. Paulsen D, Weber O, Ruebsamen-Schaeff H, et al. AIC649 induces a bi-phasic treatment response in the woodchuck model of chronic hepatitis B. PLoS One 2015;10:e0144383. [PubMed: 26656974]

30. Rodriguez-Madoz JR, Liu KH, Quetglas JI, et al. Semliki forest virus expressing interleukin-12 induces antiviral and antitumoral responses in woodchucks with chronic viral hepatitis and hepatocellular carcinoma. J Virol 2009; 83:12266–12278. [PubMed: 19740992]

31. Reimer P, Weissleder R, Brady TJ, et al. Experimental hepatocellular carcinoma: MR receptor imaging. Radiology 1991;180:641–645. [PubMed: 1871273]

32. Salem N, Kuang Y, Wang F, et al. PET imaging of hepatocellular carcinoma with 2-deoxy-2[18F]fluoro-D-glucose, 6-deoxy-6[18F] fluoro-D-glucose, [1–11C]-acetate and [N-methyl-11C]-choline. Q J Nucl Med Mol Imaging 2009;53:144–156. [PubMed: 19039303]

33. Waterhouse A, Bertoni M, Bienert S, et al. SWISS-MODEL: homology modelling of protein structures and complexes. Nucleic Acids Res 2018;46(W1): W296–W303. [PubMed: 29788355]

34. Steinegger M, Meier M, Mirdita M, et al. HH-suite3 for fast remote homology detection and deep protein annotation. BMC Bioinformatics 2019;20:473. [PubMed: 31521110]

35. Korb O, Stutzle T, Exner TE. Empirical scoring functions for advanced protein-ligand docking with PLANTS. J Chem Inf Model 2009;49:84–96. [PubMed: 19125657]

36. Julyan PJ, Taylor JH, Hastings DL, et al. SUVpeak: a new parameter for quantification of uptake in FDG PET. Nucl Med Commun 2004;25:407.

37. Bruix J, Sherman M, Practice Guidelines Committee AAftSoLD. Management of hepatocellular carcinoma. Hepatology 2005;42:1208–1236. [PubMed: 16250051]

38. Lee JH, Lee JM, Kim SJ, et al. Enhancement patterns of hepatocellular carcinomas on multiphasicmultidetector row CT: comparison with pathological differentiation. Br J Radiol 2012;85:e573–e583. [PubMed: 22919011]

39. Murakami T, Tsurusaki M. Hypervascular benign and malignant liver tumors that require differentiation from hepatocellular carcinoma: key points of imaging diagnosis. Liver Cancer 2014;3:85–96. [PubMed: 24944999]

40. Jeng LB, Changlai SP, Shen YY, et al. Limited value of 18F-2-deoxyglucose positron emission tomography to detect hepatocellular carcinoma in hepatitis B virus carriers. Hepatogastroenterology 2003;50: 2154–2156. [PubMed: 14696485]

41. Kuntz E, Kuntz HD. Hepatology: textbook and atlas. 3rd ed. Heidelberg: Springer Medizin Verlag; 2008.

42. Raveenthiran S, Esler R, Yaxley J, et al. The use of (68) Ga-PET/CT PSMA in the staging of primary and suspected recurrent renal cell carcinoma. Eur J Nucl Med Mol Imaging 2019;46:2280–2288. [PubMed: 31332498]

43. Ahn T, Roberts MJ, Abduljabar A, et al. A review of prostate-specific membrane antigen (PSMA) positron emission tomography (PET) in renal cell carcinoma (RCC). Mol Imaging Biol 2019;21:799–807. [PubMed: 30617728]

44. Nguyen DP, Xiong PL, Liu H, et al. Induction of PSMA and internalization of an anti-PSMA mAb in the vascular compartment. Mol Cancer Res 2016;14: 1045–1053. [PubMed: 27458033]

45. Aggarwal S, Ricklis RM, Williams SA, et al. Comparative study of PSMA expression in the prostate of mouse, dog, monkey, and human. Prostate 2006;66: 903–910. [PubMed: 16496413]

46. Grant CL, Caromile LA, Ho V, et al. Prostate specific membrane antigen (PSMA) regulates angiogenesis independently of VEGF during ocular neovascularization. PLoS One 2012;7:e41285. [PubMed: 22815987]

47. Liu T, Jabbes M, Nedrow-Byers JR, et al. Detection of prostate-specific membrane antigen on HUVECs in response to breast tumor-conditioned medium. Int J Oncol 2011;38:1349–1355. [PubMed: 21331445]
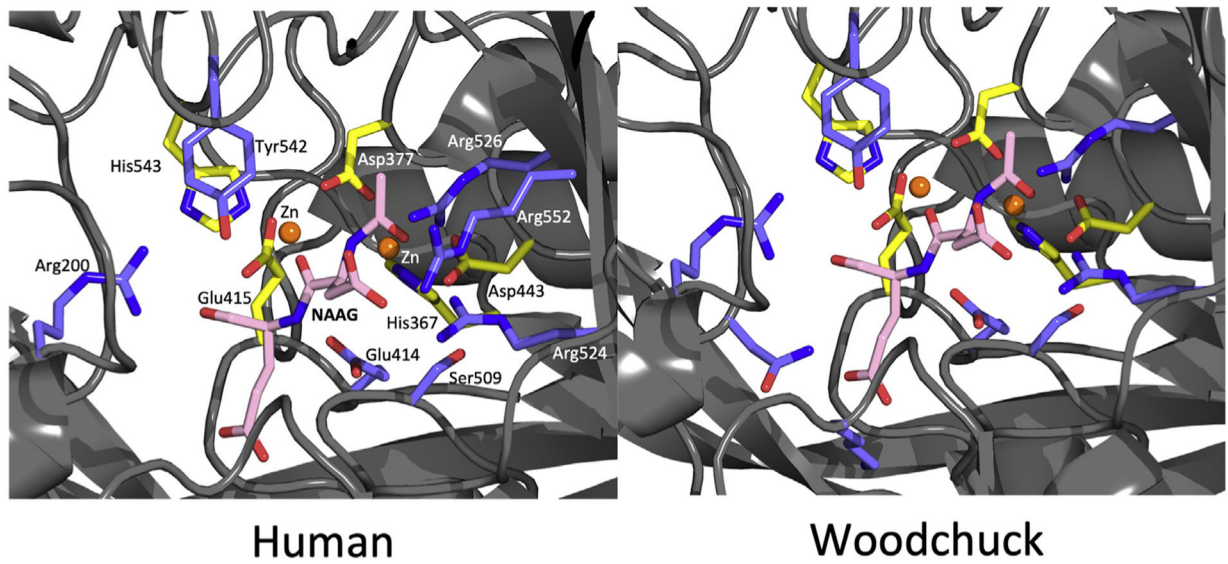
Figure 1.

The crystal structure of human PSMA (left) and a-NAAG binding complex and that of the woodchuck PSMA (right) docked with the same a-NAAG. The amino acid residues involved in ligand binding within the pocket are identical between the 2 species. Zinc is in orange. NAAG, N-acetyl-Asp-Glu.
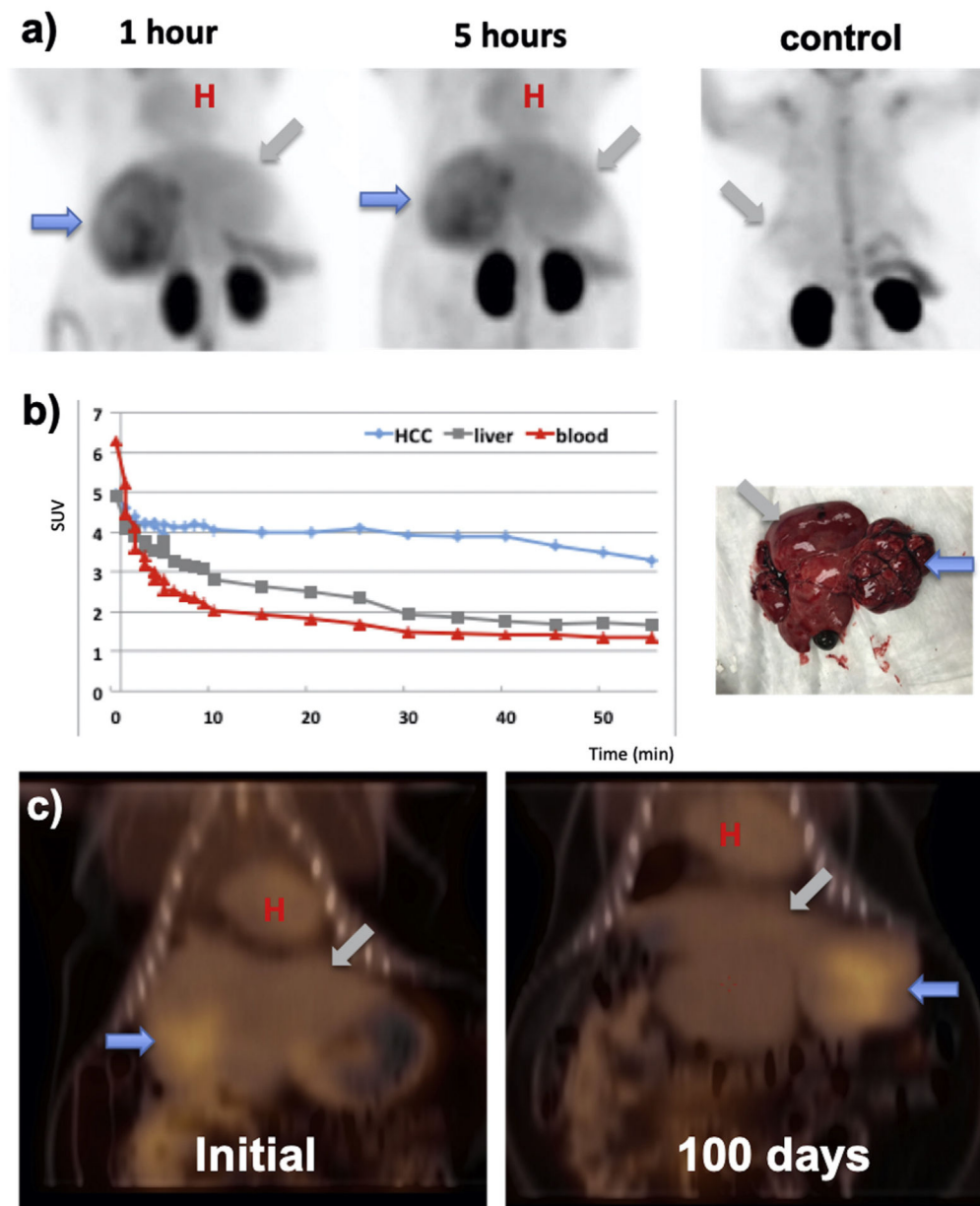
Figure 2.
PET imaging of woodchuck HCC with clinical radiotracer [^{68}Ga]PSMA-11. The blue arrows point to the heterogenic uptake in HCC; the grey arrows point to the liver. The letter **H** (red) indicates the heart. (A) sustained uptake of [^{68}Ga]PSMA-11 in HCC at 1 hour after injection of the radiotracer, and again 5 hours later in maximum intensity projection. The strong retention in kidneys is similar to the human scans with the same radiotracer (see Figure A1 right panel). A control animal without HCC was also scanned at 1 hour after injection; (B) typical time-activity curves of the radiotracer uptake, obtained during the initial 60-minute dynamic PET scan; (C) longitudinal tracking of tumor progression (100 days apart) from a coronal slice of PET/CT overlay showing a steady tracer uptake in the tumor despite HCC progression. The same tumor slipped from left to right within the

abdomen during the positioning for PET scans. The freshly excised liver with HCC after the 100-day scan was shown on the right side of (B). HCC, hepatocellular carcinoma; SUV, standardized uptake value.

a) H&E staining

b) IHC (PSMA) staining

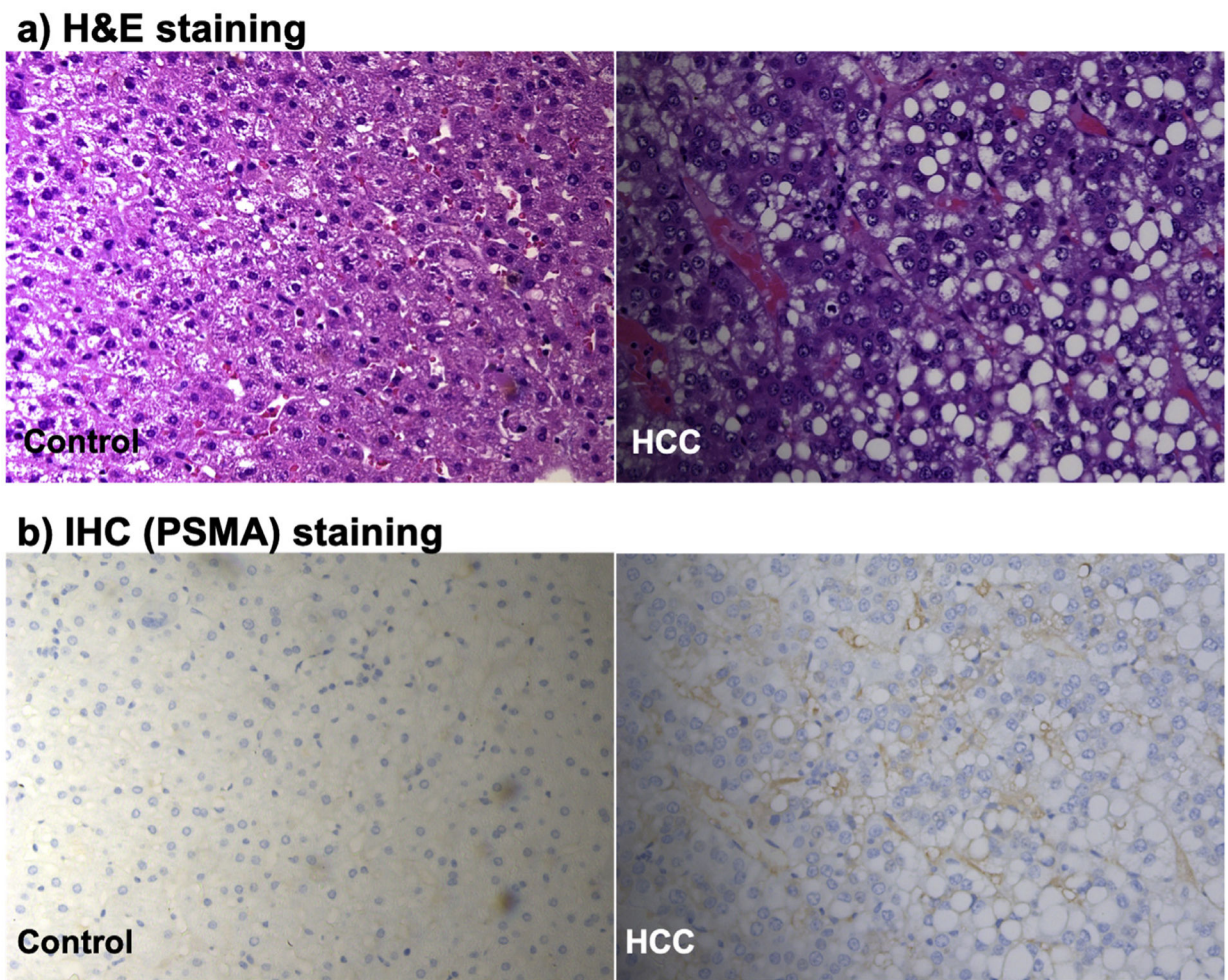**Figure 3.**
IHC staining reveals microvascular PSMA staining within the woodchuck HCC. (A) H&E staining (×20) showing mostly moderately differentiated HCC. (B) IHC staining (×20) control liver and HCC tumor with an antibody against human PSMA. H&E, hematoxylin and eosin; HCC, hepatocellular carcinoma; IHC, immunohistochemical; PSMA, prostate-specific membrane antigen.
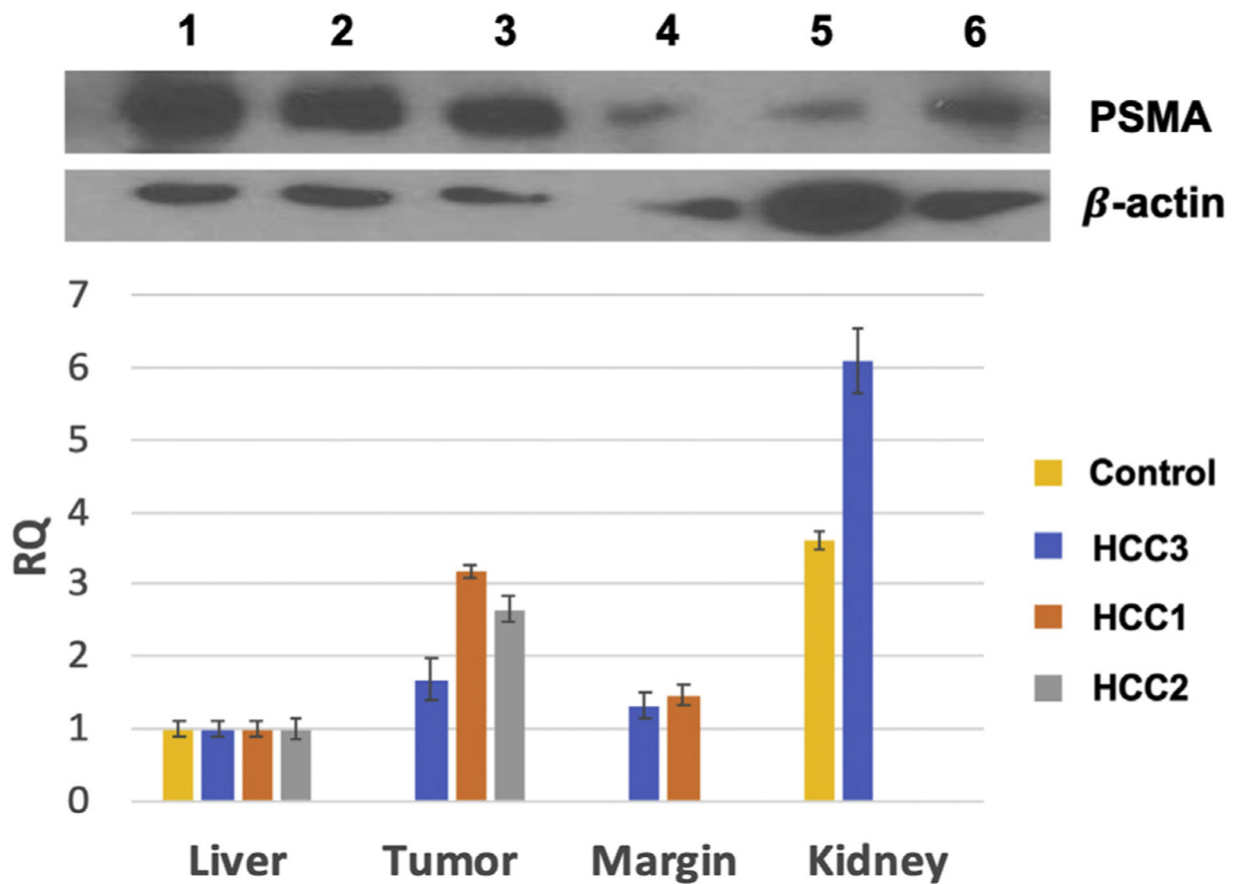
Figure 4.
Top: Western blotting using harvested tissue samples from HCC1 (**1**), HCC2 (**2**), and HCC3 (**3**) and the liver from the carrier with HCC3 (**4**), normal liver from the control (**5**), tumor margin from the carrier HCC3 (**6**), all with loading of 20 μg. The primary antibody was diluted 1:1000, and only PSMA monomers were pulled down. Bottom: qRT-PCR of PSMA expression from woodchuck tissue samples normalized to corresponding liver tissues. HCC, hepatocellular carcinoma; PSM, prostate-specific membrane; RQ, relative quantification of gene expression.

Table

Comparison of ChemPLP Docking Scores Between PSMA and Its Ligands

Species	Model ligand		
	3BXM/NAAG	4E4P/2-PMAM	5O5T/DCFPyL
Human	114.98	99.41	105.68
Woodchuck	107.52	90.29	101.04

The human 3D protein structures (3BXM, 4E4P, 5O5T) are from PDB. The woodchuck 3D homologous models were generated after the corresponding human templates, see Materials and Methods/SWISS-MODEL.